Astronomy & Astrophysics manuscript no.
(will be inserted by hand later)

Stellar population synthesis, a discriminant between gravity models

Akram Hasani Zonoozi, ⋆ Hosein Haghi, and Yousef Sobouti

Institute for Advanced Studies in Basic Sciences (IASBS), P. O. Box 45195-1159, Zanjan, Iran

Received *****; Accepted *****

Abstract. Alternative gravitations of Milgrom (MOND), of Moffat (MOG), of Sobouti (NLNL), and CDM scenarios all simulate rotation curves of spirals with reasonable details. They, however, display significant disparities in predicting the stellar mass-to-light (M_*/L) ratios of the galaxies. We maintain this feature could serve as a discriminant between different alternative theories. We analyze the rotation curves of 46 low and high surface brightness galaxies and compare the resulting M_*/Ls with the predictions of Stellar Population Synthesis (SPS) scheme. The color - M_*/L correlation obtained for MOND, and NLNL gravities are consistent with predictions of SPS models. MOG does not show such consistency, and the M_*/Ls of CDM model shows large dispersions. Furthermore, M_*/L ratios of NLNL gravity favor Kroupa's initial mass function (IMF) of SPS scheme, while those of MOND are consistent with Salpeter's IMF. Here is another indication to differentiate between different IMF's used in SPS context.

Key words. galaxies: Rotation curves– Gravitation: alternative gravities– dark matter

1. Introduction

The gravitational force of the observable mass of large astronomical systems, galaxies, clusters of galaxies, or for that matter, the universe at large, is not sufficiently strong to explain the observed dynamics of the systems. To resolve the dilemma, one main school of investigators has resorted to dark matter/dark energy scenarios. In spite of extensive efforts, however, no one has, so far, reported a direct identification of the hypothesized dark entity through non-gravitational interactions with the observable matter. This lack of direct identification has inspired an equally intensive effort to contemplate alternative theories of gravitation. The Modified Newtonian Dynamics (MOND) of Milgrom (1983), and of Bekenstein (2004), the Modified Gravity (MOG) of Moffat (2005), the Nonlocal Nonlinear (NLNL) gravity of Sobouti (2008a, b), and varieties of $f(R)$ gravities (Capozziello 2002, Capozziello et al. 2006, Capozziello et al. 2007, Carroll et al. 2004, Sobouti 2007) fall in this category.

Rotation curves of spiral galaxies as measured by the 21 cm line of HI, often extend well beyond the optical disks of the galaxies and provide a valuable body of data to determine the radial dependency of the gravitational forces in galactic scales. In this paper we construct rotation curves of a large sample of galaxies from the distribution of their detectable matter through four different gravity models, MOND, MOG, NLNL and Newtonian gravity plus cold dark matter (CDM) halos. At first glance all four models seem to reproduce the observed data with reasonable details. On a deeper examination, however, we find significant disparities in their predictions of stellar mass-to-light, M_*/L, ratios. To differentiate between the models we resort to stellar population synthesis, SPS, analysis and the color-M_*/L correlation predicted therein through various initial mass functions (IMF). There is the possibility to use this feature to discriminate between different gravity models and different IMFs.

The paper is organized as follows: In section 2 we give a brief review of different gravity models used in our analysis. In section 3 we describe our galaxy sample. Fits to the observed rotation curves are discussed in section 4. Numerical results and brief concluding remarks are given in sections 5 and 6.

2. Alternative Gravity Models

In this section we review the basic tenets of three alternative gravities as well as the Newtonian gravity plus CDM halos. We present the end formulas that we will use in the study of the dynamics of galaxies. All four accommodate the two main asymptotic features of the rotation curves of spirals; a) the slow non-**Keplerian** decline of the curves at large distances from the galaxy, and b) the Tully-Fisher (TF) relation, approximate proportionality of the asymp-

Send offprint requests to: A. Hasani Zonoozi
⋆ e-mail: a.hasani@iasbs.ac.ir

totic speed of an orbiting object to the fourth root of the mass of the galaxy (Tully & Fisher 1977).

Actually there is much debate on how fast or slow the rotation curves decline, if at all (Persic et al. 1996, Salucci et al. 2007, Gentile 2008). There are also refinements and redefinitions to the Tully-Fisher relation. McGaugh 2005 prefers to use the total baryonic (stellar + gaseous) mass in TF relation to accommodate the gas-rich galaxies. See also Stark et al. (2009), for a calibration of the baryonic TF relation with the help of gas dominated galaxies. Nonetheless, both assumptions (a) and (b), as stated above, are adequate approximations to the observed data and will be employed in this paper.

2.1. Modified Newtonian Dynamics of Milgrom, MOND

Based on observations of galactic rotation curves, Milgrom (1983), argues that the Newtonian dynamics is not viable below a certain universal acceleration, $a_0 \simeq 1.2 \times 10^{-10}\mathrm{m/sec}^2$. To comply with the Tully-Fisher relation he modifies the law of motion to have an acceleration proportional to the square root of the Newtonian acceleration. MOND's acceleration, g_{mond}, and the Newtonian one, g_N, are connected through Eq. (1) below

$$\frac{g_{mond}}{a_0}\ \mu\left(\frac{g_{mond}}{a_0}\right) = \frac{g_N}{a_0}, \tag{1}$$

where $\mu(x)$ is an interpolating function for transition from the Newtonian to the MONDian regime. It runs smoothly from $\mu(x) = x$ for $x << 1$ to $\mu(x) = 1$ for $x >> 1$. Here we adopt two commonly used such functions, the standard interpolating function of Bekenstein & Milgrom (1984):

$$\mu_1(x) = \frac{x}{(1+x^2)^{1/2}}, \tag{2}$$

and the simpler function of Famaey & Binney (2005),

$$\mu_2(x) = \frac{x}{1+x}. \tag{3}$$

Hereafter, analysis using μ_1 and μ_2 will be refereed to as MOND1 and MOND2, respectively.

2.2. Nonlocal Nonlinear Gravity, NLNL

This is a review from Sobouti (2008a, b, 2009) and Sobouti et al. (2009). One begins with a spacetime pervaded by a baryonic perfect fluid of known density and pressure and a hypothetical dark companion. In the baryonic vacuum one solves the GR field equations in terms of the unknown density and pressure of the dark companion. In the weak field regime one then requires the asymptotic gravitational force to comply with the TF relation. This enables one to obtain the spatial distribution of the dark density. For asymptotically flat rotation curves the amplitude of the dark density turns out to be proportional to the square root of the total mass of the baryonic system. The dark pressure is obtained from the hydrostatic equilibrium of the dark fluid, itself a requirement of the **Bianchi** identities. For the gravitational acceleration, g_{nlnl}, outside a spherically symmetric baryonic system one finds

$$\frac{g_{nlnl}}{a_0} = \left(\frac{g_N}{a_0}\right)^{1/2} + \left(\frac{g_N}{a_0}\right)\cdots + \lambda_n\left(\frac{g_N}{a_0}\right)^{(n+1)/2}\cdots, \tag{4}$$

where g_N and a_0 are the the Newtonian and Milgrom's accelerations, respectively, and $\lambda_n,\ n \geq 2$, are dimensionless parameters to be addressed shortly. The first term on the right hand side of Eq. (4) is a direct consequence of the TF relation. The second term is the classical Newtonian acceleration. The remaining terms come from a formal solution of the field equations. To the best knowledge of the authors the extent and precision of the present day data on the rotation curves of spirals do not allow meaningful estimates of λ_n. They, however, are bound to be small. For as we shall see later, the first two terms of Eq. (4) reproduce the observed curves with adequate details. Moreover, the $n = 2$ term alone in Eq.(4) fades away as r^{-3}, in the same way the quadrupole field of a flattened system does. This means, before considering the third term, one should worry about the non-sphericity of the galaxy. In view of these considerations, hereafter, we shall truncate the series of Eq. (4) at its second term.

Equation (4) is an exact weak field solution of GR outside the baryonic system. The solution inside the system is obtained by requiring continuity of the gravitational acceleration at the boundary of the system. This leads to an expression of the same form as Eq. (4), where now $g_N = GM(r)r^{-2}$, and $M(r)$ is the mass inside the sphere of radius r.

The weak field limit of Tensor-Vector-Scalar (TeVeS) gravity of Bekenstein (2004) is known to produce MOND. With Bekenstein's interpolating function

$$\mu_3(x) = \frac{(1+4x)^{1/2}-1}{(1+4x)^{1/2}+1}, \tag{5}$$

MOND's acceleration gives the first two terms of Eq. (4), (see also Hernandez et al. (2010)). **In this sense one might consider the truncated version of Eq. (4) as a test of MOND with the interpolating function of Eq. (4).** This is a coincidence, however, and it occurs **only** in the weak field limit of both TeVeS and NLNL theories.

The dependence of the gravitational force of Eq. (4) on its source, the baryonic density $\rho(r)$, is *nonlinear*, and through the integral $M(r) = \int \rho d^3x$, is *nonlocal*, hence the acronym *Nonlocal Nonlinear*. In spite of its dark matter beginning, the theory does not advocate a dark matter point of view. The non-Newtonian term in Eq. (4) could be interpreted as a modification of the standard gravitation.

Equation (4) has an empirical basis and is designed to accommodate spherically symmetric systems. Like all other alternatives discussed in this paper, its extension to non-spherical and many body systems is a non-trivial issue and may require further assumptions not contemplated so far. Nonetheless, we are working on one such extension

and hope to be able to have a sensible generalization of the virial theorem and possibly a hint to the so-called fundamental plane of clusters of galaxies.

Our anonymous referee points out, while NLNL has a covariant beginning, a) M in Eq. (4) is not a covariant scalar, and b) appearance of $M^{1/2}$ limits the theory to a given system of mass M, preventing generalization to the whole unverse, say. Our response to point (a) is at one stage we have resorted to the weak field approximation. There the question of covariance does not arise and M is a scalar in the non-relativistic sense of the word. As to point (b), We note that nonlinearity and nonlocality are the ever-present feature of any and all approaches to galactic rotation curves that have been offered so far. This makes them incapable of generalization to problems beyond the galaxies. All we are doing here is to draw attention to these two features and the peculiarities associated with it. This includes "one theory for one system" as the referee correctly puts it.

One last remark: Hehl & Mashhoon 2009 have a novel and sophisticated approach to nonlocal gravity. In a galactic context and in the weak field regime, they are able to produce flat rotation curves but not the Tully-Fisher relation, i.e. nonlinear dependence on the total mass of the galaxy. Blome et al. 2010 revisit the problem and make provision for some sort of nonlinearity that in principle could be adjusted to give the Tully-Fisher relation.

2.3. Modified Gravity of Moffat, MOG

MOG consists of three theories of gravity: the nonsymmetric gravity theory (NGT), the metric-skew-tensor gravity (MSTG) theory, and the scalar-tensor-vector gravity (STVG). They rely on the existence of a massive vector field universally coupled to matter. Moffat maintains that MOG explain the rotation curves of galaxies, clusters of galaxies and cosmological issues without resorting to dark matter (Moffat 1995, Moffat 2005, Moffat 2006, Moffat & Toth 2009). Good fits to astrophysical and cosmological data have been obtained with his recent version of STVG. One notable feature of NGT, MSTG, and STVG is that the modified acceleration at weak gravitational fields has a Yukawa type addition to the Newtonian acceleration. In the weak field limit, STVG, NGT and MSTG produce similar results. The recipe for the gravitational force of a spherically distributed mass, $M(r)$, is (Moffat 2006)

$$g_{mog} = \frac{G(r)M(r)}{r^2}, \tag{6}$$
$$G(r) = G_N \times \left\{1 + \alpha(r)\left[1 - e^{-r/r_0}\left(1 + \frac{r}{r_0}\right)\right]\right\},$$

where G_N is the Newtonian gravitational constant, $M(r)$ is the baryonic mass inside the radius r, and $\alpha(r) = [M_0/M(r)]^{1/2}$. The parameters M_0 or r_0 determine the coupling strength of the vector field to the baryonic matter and to the range of the force, respectively. They are not universal constants and vary with the size of the systems (Brownstein & Moffat 2006, Haghi & Rahvar 2010). In galactic scales, they are determined by analyzing the best fit of the theory to the rotation curves of LSB and HSB galaxies. For normal size galaxies, they are reported as $M_0 = 9.6 \times 10^{11} M_\odot$ and $r_0 = 13.9$ kpc, and for dwarf galaxies, as $M_0 = 2.4 \times 10^{11} M_\odot$ and $r_0 = 9.7$ kpc (Moffat 2006). An empirical fitting of M_0 versus r_0 for a wide range of spherically symmetric systems, from solar size systems to clusters of galaxies is depicted in Figure 2 of (Brownstein & Moffat 2006). MOG's gravitation tends to the Newtonian one as $M_0 \to 0$ and $r_0 \to \infty$.

2.4. Newtonian Gravity plus Cold Dark Matter, CDM

In this scenario, gravitation is Newtonian. To account for the nonclassical behavior of the rotation curves one adds a spherically symmetric dark halo to the galaxy. **Here, we consider NFW halo with the density distribution,**

$$\rho_{NFW}(r) = \frac{\rho_s}{(r/r_s)(1 + r/r_s)^2},$$

and the gravitational acceleration

$$g_{NFW} = 4\pi G \rho_s r_s (\frac{r_s}{r})^2 \left[\ln\left(1 + \frac{r}{r_s}\right) - \frac{r/r_s}{(1 + r/r_s)}\right], \tag{7}$$

where r_s and ρ_s are the characteristic radius and density of the distribution (Navarro, Frenk & White 1996). The NFW density comes from numerical simulations of ΛCDM theory in the framework of structure formation. There, one also finds that these parameters are correlated to each other with the following relations, leaving only one free parameter to characterize the halo (see Bullock et al. 2001, Wechsler et al. 2002, and Neto et al. 2007 for details). Thus,

$$\rho_s = \frac{\Delta}{3} \frac{c^3}{ln(1 + c) - c/(1 + c)} \rho_c, \tag{8}$$

$$c = 13.6 \left(\frac{M_{vir}}{10^{11} M_\odot}\right)^{-0.13}, r_s = 8.8 \left(\frac{M_{vir}}{10^{11} M_\odot}\right)^{0.46} kpc, \tag{9}$$

where ρ_c is the critical density of the Universe and $\Delta = 200$ is the virial overdensity at z=0 (Bryan & Norman 1998).

Before we leave this section let us point out some of the shortcomings of the models discussed here.

All fail to go beyond the point mass or at most a spherically symmetric mass distribution.

At their final formulation, all resort to the Tully-Fisher relation to fix their free parameters.

This limits their applicability to spirals only, and that with the approximation of spherical symmetry.

All fail to address 'many body problems', e.g. Milky Way-Andromeda pair, clusters of galaxies, etc. Even, if they claim they do so, their observational verification remains to be seen.

All fail to pass solar system tests.

All produce some excess lensing but not enough to accommodate observations. To see this it is sufficient to note that the dark matter equivalent of the model produces an excess gravitation. See also Mendoza & Rosas-Guevara 2007.

None should be expected to throw light on any cosmological questions such as CMB power spectrum, etc, for they are designed only for galactic missing-mass/missing-gravity issues.

Accuracy and extent of the existing data is a limiting factor for refinements on any of the models.

3. Observational data

There are diverse morphological types of galaxies with diverse shapes and sizes to their rotation curves. Our sample, a collection of 46 galaxies taken from Sanders (1996), McGaugh & de Blok (1998), Sanders & Verheijen (1998) and Begeman (1991), accommodates these diversities. Members of the sample have well measured rotational speeds and accurate surface photometry. They are listed in Table 1 and shown in Figs. 1 - 3. The sample includes several very large and luminous members with well-extended rotation curves, e.g., UGC 2885, NGC 801 & NGC 2903. They have high surface brightness (HSB), massive stellar component, and low gas content. Typically, their rotation curve rises steeply to a maximum and declines slowly into an almost horizontal asymptote. There are also a number of dwarf, gas-dominated and low surface brightness (LSB) galaxies, e.g. DDO 168. There is no conspicuous maximum, and in some galaxies not even a flat asymptote, to their rotation curve. It is generally believed that deviations from the classical dynamics is more pronounced in LSBs than in HSBs. (McGaugh & de Blok 1998a, Sanders & Noordermeer 2007, Gentile et al. 2010)

Twenty-eight members of the sample, of both HSB and LSB types, are located in the Ursa **Major** cluster of galaxies, believed to be at the distance of about 15.5 Mpc (Tully & Verheijen 1997). Seven of the galaxies, listed in Table 3, have central bulges and are treated differently, to be explained shortly. For a full description of the sample the interested reader is referred to Sanders and McGaugh (2002).

4. Constructing rotation curves

We calculate the rotation speed of a test object circling the galaxy as a function of distance from the galactic center and the distribution of the detectable matter in the galaxy. The procedure we follow is almost that of Sanders and McGaugh (2002):

We approximate the galaxy by a spherically symmetric system. **The error committed amounts to ignoring the quadrupole field of the flattened galaxy. At a distance r, it is of the order of $(R_{gyr}/r)^2$, where R_{gyr} is the gyration radius of the galaxy about its axis of symmetry.** In systems, such as Kuzmin's, Mestel's, Miyamoto - Nagai's, and exponential disks (Binney & Tremaine 1987), R_{gyr} is a few tenths of the typical length scale of the galaxy. **At distances of about 2-3 times the galaxy's visible disk the ratio $(R_{gyr}/r)^2$ drops to about few percent. See Binney & Tremaine (1987), equations (2-165, 2-166), and figure (2-17) for further details.**

We assume a constant M_*/L ratio, throughout the galaxy, though this is not strictly the case, because of the color gradient in spiral galaxies. However, in seven bulged spirals we find assigning different M_*/L to the bulge and the disk improves fittings to the observed data.

We assume the HI gas is in co-planer rotation about the center of the galaxy, an assumption which may not hold in galaxies with strong bars (Sanders & McGaugh 2002).

Given the observed distribution of the baryonic matter (stellar and gaseous disks, plus a spheroidal bulge, if present), the effective radial gravitational force, and subsequently the circular speed, is calculated from Eqs. (1) and (4) - (7). Fitting of the calculated rotation curves to the observed data points is achieved by adjusting the M_*/L ratio, through a least-square χ^2, defined as

$$\chi^2 = \frac{1}{N}\sum_{i=1}^{N}\frac{(v^i_{theory} - v^i_{obs})^2}{\sigma_i^2}, \tag{10}$$

where σ_i is the observational uncertainty in the rotation speeds. The M_*/L ratio of the disk and of the bulge are our ultimate results.

5. Numerical Results

All models trace the observed data with reasonable details. The best-fit χ^2 and M_*/L values are listed in Table 1. Figures 1 - 3 show fits of theoretically constructed rotation curves to the observations of 46 galaxies. The general trend of HSB curves (steep rise to a maximum followed by gradual decline to an almost flat asymptote), and of LSB curves (slow rise often with no asymptote in sight) are evident.

Seven galaxies have prominent bulge components. One expects a bulge with an older population of stars to have a higher M_*/L ratio than a disk with a younger population. Therefore, to obtain a better fit for these galaxies, we have allowed the model to choose different M_*/Ls for the disk and the bulge. The result, shown in Table 2, confirms the expectation. The minimum χ^2s of Table 2 are detectably lower than those of the corresponding entries of Table 1 obtained by a single M_*/L fit. Nevertheless, one galaxy

in our model, NGC 801, and four in MOND's, NGC 801, NGC 5371, UGC 2885 and NGC 5907, predict untenably lower M_*/L for the bulge than for the disk.

McGaugh (private communication) advises us that this oddity might partially be due to the low resolution of HI data and/or the sharp rise of $v(r)$ in the bulge. If $v(r)$ is not quite resolved, one tends to underestimate it, and the M_*/L of the bulge with it. In many of these galaxies it is indeed not obvious, whether the inner component is really a "bulge" in the classical sense of a 3D component with an $r^{1/4}$ profile. It is also said that neglecting the flattening of a bulge leads to an error in its mass-to-light ratio (Noordermeer 2008). In NGC 6946, there is a tiny bulge (4 percent of the total light in B-band). It is **predicted** as a little kinematic bump in the inner 1 kpc, in high resolution **Fabry-Pérot data (Blais-Ouellette et al. 2004)**. Moreover, HI distribution in NGC 6946 is not symmetric in the galactic plane. It is patchy and seems to deviate from circular orbits (Carginan et al. 1990).

Ten entries in Table 1 have unacceptably large χ^2s. Suspecting the failure of the assumption of constant M_*/L, we have followed Barnes et al. (2007), and examined a radially varying, $M_*/L = (M_*/L)_0 + mr$. The best fit values of the constants $(M_*/L)_0$ and m for some of them are displayed in Table 3. The slope, m, is much too small to result in appreciably lower χ^2. The root of the failure should lie elsewhere. For example, the assumption of cold unobservable molecular gas in the galactic disk (Tiret & Combes 2009) leads to better fits with lower χ^2.

6. Color – M_*/L Correlation

How realistic **are** the inferred M_*/L ratios? Stellar population synthesis (SPS) models predict a linear relation between colors and M_*/L ratios. Redder galaxies should have larger M_*/L (see, e.g., Bell & de Jong 2001, Bell et al. 2003, Portinari et al. 2004). The slope of this linear relation does not depend on exact details of the history of star formation, i.e. the assumed IMF. But, depending on how many stars are present at the low-mass end of the stellar IMF, the color-M_*/L curve shifts up and down. For low mass stars contribute significantly to the mass of a population, but not so much to its luminosity and color (Bell & de Jong 2001).

In SPS scheme Salpeter's (1955) IMF overestimates the M_*/L ratios of many of the galaxies and violates the condition of 'disk mass less than the mass of maximum disk'. To remedy the case, Bell et al. (2003) scale down Salpeter's IMF and come up with a limit for the color-M_*/L relation above which the physical viability is not guaranteed. Their suggested relation is

$$\log(M_*/L_B) = 1.74(B-V) - 0.94. \quad (11)$$

There are other IMF's leading to slightly different relations. **For example, Bottema (1997) argue for a substantially submaximal M/L ratio for all disk dominated galaxies based on an analysis of the vertical velocity dispersion of stars.** Kroupa (2001), introduces a turnover at the low mass end of his IMF. The slope 1.74 is insensitive to such variations in IMF, but the y-intercept is. To obtain the equivalent relation for standard Salpeter's, Kroupa's, and Bottema's IMF one should shift Eq. (11) and the plots in Figure (4) up and down by roughly (0.15, -0.15, -0.35) dex, respectively (Bell et al. 2003).

In Figure 4, we contrast M_*/L ratios of the four gravity models against the predictions of SPS. **We used the B-band luminosities from Sanders & McGaugh (2002).** In each frame the solid line is the best fit to the data points obtained from the analysis of the rotation curves. The theoretical SPS predictions of Bell & de Jong 2001, and Bell et al. 2003, for different IMFs are also plotted. The slope of NLNL, 1.75 ± 0.26, of MOND1, 1.78 ± 0.23, and of MOND2, 1.81 ± 0.21 are reasonably close to that of Eq. (11). The corresponding y-intercepts, -1.13 ± 0.15, -0.88 ± 0.14, and -1.06 ± 0.12, respectively, are also in harmony with that of Eq. (11). **The uncertainties in slopes and y-intercepts are in the 1-σ error.** The errors in y-intercepts are small enough to enable one to differentiate between different IMFs. NLNL is in good agrement with Kroupa's IMF. MOND1 falls somewhere between standard Salpeter's and scaled Salpeter's IMF. MOND2 agrees with Kroupa's and scaled Salpeter's IMF.

The slope for MOG, 1.06 ± 0.21, cannot be reconciled with SPS predictions. **However, the slope of NFW halo, 2.33 ± 0.67, is consistent within the error with 1.74, dispersion of the simulated data points in this case is too large to draw meaningful correlation between color and M/L ratios.**

Any alternative gravity can have a dark matter equivalent. Deviations from the Newtonian gravity can be attributed to a hypothetical entity and a dark density profile can be calculated through Poisson's equation, say. One feature, however distinguishes such an interpretation from the conventional CDM scenarios. Here, there is a well defined relation between the baryonic matter and its so-interpreted dark companion. In CDM models baryonic and dark matters may co-exist independently. In our opinion, the reason for good agreement of NLNL and MOND gravities with SPS predictions and non-compliance of CDM with it lies in the existence or non-existence of this relation between the observable and non observable matters . In NLNL and MOND, baryonic matter plays a pivotal role and dark entity owes its existence to it. This is not the case in CDM. Dark matter is allowed to play **a** role independently from the observable matter. As for MOG, we are not in a position to express an opinion.

Let us summarize our conclusion: a) the SPS scheme can differentiate between different gravity models and b) the two together can choose between different IMFs. The mere fact that a gravity theory reproduces the observed rotation curves satisfactorily does not tell the whole story.

7. Concluding Remarks

At least on galactic scales, dynamics of spirals casts doubt on the viability of the classical theories of gravitation. A number of alternative theories are capable of reproducing the rotation curves of spirals with acceptable details, a nontrivial fact that deserves attention. In this paper we use three alternative theories of gravitation, MOND, MOG, NLNL, and a CDM model to deduce the dynamics of a good size sample of high and low surface brightness galaxy types, and check the results against observations. The models, in spite of the fact that all simulate the rotation curves in more or less to the same degree of accuracy, are not equivalent.

In MOND, MOG, and NLNL, rotation curves are constructed with only one free adjustable parameter, the stellar mass-to-light ratio. This is in contrast to the CDM model, where an additional parameter is needed to describe the dark component.

It must be stressed that the assumption of spherical symmetric distribution for spiral galaxies in NLNL and MOG models is a limitation of the present study.

There are cases of bulged galaxies where fits to observations lead to lower M_*/L ratios for the bulge than for the disk. This might be due to the low resolution of HI data and of inner $v(r)$, and/or uncertain size of the bulge.

Stellar population synthesis models impose constrains on M_*/L: Redder galaxies should have larger M_*/L ratios. NLNL and MOND fulfill this expectation, albeit with different IMFs. This is noteworthy, as there is no explicit/implicit connection between the basic tenets of the SPS and NLNL and/or MOND. **On the other hand MOG does not meet the SPS constraints, and the M_*/Ls of CDM model shows large scattering such that does not show meaningful correlation between color and M/L ratios. It should be noted that, since the weak field limit of NLNL is similar to MOND with interpolation function μ_3, this is actually an effective test of Bekenstein's MOND interpolating function.**

SPS predictions of M_*/L ratios are sensitive to the adopted IMF. The M_*/L ratios inferred from Salpeter's IMF are notably larger than those obtained from Kroupa's. NLNL favors Kroupa's IMF, which produces lower M_*/L, implying lesser disk masses.

Last but not least: both MOND and our proposed Nonlinear Nonlocal gravitation have empirical beginnings and rely heavily on the Tully-Fisher relation, itself an empirical finding.

Acknowledgements. Stacy McGaugh provided us with their recent data on rotation curves. We thank him and also Eric Bell, Roelf de Jong, Mohammad Dehghan Niry, and Pavel Kroupa for their useful comments.

References

Barnes, E. I., Kosowsky, A., and Sellwood, J. A. 2007, AJ, 133, 1698
Begeman, K. G., Broeils, A. H., and Sanders, R. H. 1991 MNRAS, 249, 523
Bekenstein, J. D., and Milgrom, M., 1984 ApJ, 286, 7
Bekenstein, J. D. 2004, Phys. Rev. D, 70, 083509
Bell E. F., and de Jong R. S. 2001, ApJ, 550, 212
Bell, E. F., McIntosh, D. H., Katz, N., and Weinberg, M. D. 2003, ApJS, 149, 289
Binney J., and Tremaine, S. 1987, Galactic Dynamics, Princeton Univ. Press, Princeton, NJ.

Blome, H. J., Chicone, C., Hehl, F. W., Mashhoon, B., 2010, Phys. Rev. D81:065020

Blais-Ouellette, S., Amram, P., Carignan, C., and Swaters, R., 2004, A&A, 420, 147

Bottema, R., 1997, A&A, 328, 517

Bryan, G. L., Norman, M. L. 1998, ApJ, 495, 80
Brownstein, J. R., and Moffat, J. W. 2006, ApJ, 636, 721
Brownstein, J. R. and Moffat, J. W., (astro-ph/0702146).
Bullock, J. S., Kolatt, T. S., Rachel, Y. S., Somerville, S., Kravtsov, A. V., Klypin, A. A., Primack, J.R., Dekel, A. 2001, MNRAS, 321, 559
Capozziello, S. 2002, Int. J. Mod. Phys. D., 11, 483
Capozziello, S., Cardone, V. F., and Troisi, A. 2006, JCAP, 8, 1
Capozziello, S., Cardone, V. F., and Troisi, A. 2007, 375, 1423
Carignan, C., Charbonneau, P., Boulanger, F., & Viallefond, F. 1990, A&A, 234, 43
Carroll, S., Duvvuri, V., Trodden, M., and Turner, M. 2004, Phys. Rev. D, 70, 2839
Famaey & Binney 2005, MNRAS, 363, 603
Gentile, G., 2008, ApJ, 684, 1018
Gentile, G., Baes, M., Famaey, B., and Van Acoleyen, K., 2010, arxiv:1004.3421
Haghi, H., and Rahvar, S. 2010, IJTP, 49, 1004

Hehl, F. W., Mashhoon, B., 2009 Phys. Lett. B673:279-282
Hernandez, X., Mendoza, S., Suarez, T., Bernal, T., arXiv:0904.1434
Kroupa, P., 2001 MNRAS, 322, 231.
McGaugh, S. S., and de Blok, W. J. G. 1998, ApJ, 499: 41-65
McGaugh, S. S., and de Blok, W. J. G. 1998, ApJ, 499: 66-81
McGaugh, S. S., 2005, ApJ, 632, 859

Mendoza, S., Rosas-Guevara, Y. M., 2007, A&A, 472, 367-371
Milgrom, M. 1983, ApJ, 270, 365
Moffat, J. W. 1995 Phys. Letts. B, 355, 447
Moffat, J. W., 2005, JCAP 2005, 003
Moffat, J. W. 2006, JCAP, 2006, 004
Moffat, J. W., Toth, V. T. 2009, ApJ, 680:1158.
Navarro, J.F., Frenk, C.S.,White, S.D.M. 1996, ApJ, 462, 563
Neto, A. F., et al. 2007, MNRAS, 381, 1450
Noordermeer, E. 2008, MNRAS, 385, 1359
Persic, M., Salucci, P., Stel, F. 1996, MNRAS, 281, 27
Portinari, L., Sommer-Larsen, J., and Tantalo, R. 2004, MNRAS, 347, 691

Salpeter, E. E. 1955, ApJ, 121, 161.
Salucci, P., Lapi, A., Tonini, C., Gentile, G., Yegorova, I., & Klein, U. 2007, MNRAS, 378, 41
Sanders R. H. 1996, ApJ, 473, 117
Sanders, R. H., and Verheijen M. A. W., 1998, ApJ, 503, 97-108
Sanders R. H., and McGaugh S. S. 2002, ARA&A, 40, 263
Sanders, R. H., & Noordermeer, E. 2007, MNRAS, 379, 702
Sobouti, Y. 2007, A&A, 464, 921
Sobouti, Y. 2008a, arXiv:0810.2198[gr-qc]; 2008b, arXiv:0812.4127v2 [gr-qc]
Sobouti, Y. 2009, arXiv:0903.5007 [gr-qc]
Sobouti, Y., Hasani Zonoozi, A., and Haghi, H. 2009, A&A, 507, 635, arxiv:0906.0668[gr-qc] (paperI)
Stark, D. V., McGaugh, S. S., Swaters, R. A. 2009, AJ, 138, 392
Tiret, O., and Combes, F. 2009, A&A, **496**, 659
Tully, R. B., and Fisher, J. R. 1977, A&A, **54**, 661
Tully, R. B., & Verheijen, M. A. W. 1997, ApJ, 484, 145
Wechsler, R. H., Bullock, J. S., Primack, J. R., Kravtsov, A. V., Dekel, A. 2002, ApJ, 568, 52

Galaxy (Type)	B-V	M^*/L NLNL	χ^2 NLNL	M^*/L Mond1	χ^2 Mond1	M^*/L Mond2	χ^2 Mond2	M^*/L MOG	χ^2 MOG	M^*/L NFW	χ^2 NFW
HSB Galaxies											
M 33 (Sc)	0.55	0.3	39.25	0.6	30.22	0.4	36.47	0.8	45.03	0.2	125.00
NGC 300 (Sc)	0.58	0.4	2.35	0.7	2.26	0.5	2.51	1.3	2.54	0.1	2.94
NGC 2903 (Sc)	0.55	1.7	4.79	3.0	6.07	2.2	5.72	2.4	7.18	2.4	3.60
NGC 3726 (SBc)	0.45	0.5	4.60	1.0	3.47	0.7	3.86	0.9	5.00	0.6	3.03
NGC 3769 (SBb)	0.64	0.7	0.70	1.2	0.75	0.9	0.65	1.4	1.06	0.7	0.42
NGC 3877 (Sc)	0.68	0.9	2.60	1.7	2.66	1.2	2.62	1.5	3.07	1.1	2.51
NGC 3893 (Sc)	0.56	1.0	1.88	1.7	4.12	1.3	2.11	1.6	2.76	1.2	1.89
NGC 3949 (Sbc)	0.39	0.5	3.97	0.8	5.34	0.6	3.88	0.8	5.00	0.5	3.29
NGC 3953 (SBbc)	0.71	1.5	0.47	2.7	1.13	2.0	0.48	2.2	0.44	2.1	1.05
NGC 3972 (Sbc)	0.55	0.8	3.08	1.5	3.22	1.0	3.03	1.6	2.85	0.2	1.25
NGC 3992 (SBbc)	0.72	2.7	1.02	4.9	0.65	3.6	0.88	3.6	2.08	4.5	4.11
NGC 4013 (sb)	0.83	1.8	2.24	3.1	1.37	2.3	1.62	2.7	2.05	2.2	1.63
NGC 4051 (SBbc)	0.62	0.7	0.90	1.2	0.88	0.9	0.78	1.1	0.76	0.7	0.78
NGC 4085 (Sc)	0.47	0.6	6.03	1.1	6.84	0.8	6.02	1.1	6.94	0.5	3.93
NGC 4088 (Sbc)	0.51	0.6	1.75	1.1	1.49	0.8	1.62	1.0	1.97	0.8	1.24
NGC 4100 (Sbc)	0.63	1.3	1.58	2.4	2.07	1.8	2.02	2.1	2.12	1.7	2.06
NGC 4138 (Sa)	-	2.0	0.81	3.5	1.61	2.7	0.98	3.2	1.20	2.9	1.09
NGC 4157 (Sb)	0.66	1.3	0.87	2.4	0.92	1.7	0.85	2.0	0.84	1.7	0.89
NGC 4217 (Sb)	0.77	1.2	2.90	2.2	3.95	1.6	2.92	1.9	2.63	1.5	3.02
NGC 4389 (SBbc)	-	0.2	5.57	0.4	5.36	0.3	5.42	0.6	6.33	0.1	4.33
NGC 5585 (SBcd)	0.46	0.3	10.46	0.5	10.43	0.4	10.22	1.1	16.87	0.1	19.03
NGC 6946 (SABcd)	0.40	0.3	21.61	0.5	11.46	0.4	17.90	0.5	31.75	0.3	1.01
NGC 7793 (Scd)	0.63	0.6	1.48	1.2	1.48	0.9	1.44	1.5	1.02	0.8	1.91
UGC 6399 (Sm)	-	0.6	0.10	1.0	0.16	0.8	0.17	1.8	0.04	0.1	1.48
UGC 6973 (Sab)	-	1.7	10.57	2.7	20.46	2.2	11.81	2.6	20.24	2.0	6.48
NGC 801^b (Sc)	0.61	0.8	14.15	1.2	23.14	1.0	14.75	1.2	23.90	1.2	49.61
NGC 2998^b (SBc)	0.45	0.7	2.96	1.2	2.64	0.9	2.43	1.0	2.35	1.4	6.80
NGC 5371^b (S(B)b)	0.65	0.9	6.93	1.6	10.02	1.2	8.32	1.3	6.65	1.5	7.65
NGC 5533^b (Sab)	0.77	2.1	1.11	3.3	2.33	2.6	1.61	3.8	8.50	5.6	19.61
NGC 5907^b (Sc)	0.78	2.1	4.27	4.0	2.93	2.8	3.82	3.0	6.10	3.5	11.23
NGC 6674^b (SBb)	0.57	1.6	6.64	2.7	10.96	2.0	7.65	2.6	41.06	4.1	66.96
UGC 2885^b (Sbc)	0.47	0.9	3.04	1.5	2.80	1.2	2.98	1.4	6.64	1.9	14.85
LSB Galaxies											
DDO 168 (SO)	0.32	0.1	21.56	0.2	11.50	0.1	14.35	1.5	14.64	0.1	26.67
NGC 247 (SBc)	0.54	0.7	4.16	1.1	3.71	0.8	3.91	2.0	3.74	0.1	10.34
NGC 1560 (Sd)	0.57	0.3	1.52	1.1	3.35	0.6	1.94	4.6	10.56	0.1	17.00
NGC 3917 (Scd)	0.60	0.7	4.58	1.3	4.49	0.9	4.58	1.4	4.03	0.2	6.51
NGC 4010 (SBd)	0.54	0.8	1.76	1.4	1.81	1.0	1.74	1.7	1.16	0.1	2.42
NGC 4183 (Sa)	0.39	0.4	1.09	0.7	0.98	0.5	0.98	1.0	1.54	0.4	0.20
UGC 128 (Sdm)	0.60	0.6	0.63	1.1	0.48	0.8	0.54	1.9	0.36	0.1	2.57
UGC 6446 (Sd)	0.39	0.3	4.49	0.5	2.30	0.4	3.29	1.2	2.35	0.1	0.30
UGC 6667 (Scd)	0.65	0.6	0.69	1.0	0.94	0.8	0.88	1.9	0.59	0.1	3.95
UGC 6917 (SBd)	0.53	0.8	0.72	1.4	0.64	1.0	0.69	2.0	0.84	0.1	0.49
UGC 6923 (Sdm)	-	0.4	1.03	0.8	1.17	0.6	1.16	1.4	2.28	0.1	0.56
UGC 6930 (SBd)	0.59	0.4	0.54	0.8	0.28	0.6	0.34	1.2	0.34	0.2	0.19
UGC 6983 (SBcd)	0.45	0.9	1.68	1.7	1.30	1.2	1.46	2.3	1.90	1.1	0.54
UGC 7089 (Sdm)	-	0.1	0.25	0.2	0.14	0.2	0.40	0.6	0.11	0.9	3.18

Table 1. Best-fit reduced χ^2 and M_*/L values of 32 HSB galaxies in NLNL, MOND, MOG, and **NFW** models. Hubble types are from NASA/IPAC Extragalactic Database (NED). Bulged galaxies are marked by a superscript '^{b}'.

Galaxy	χ^2_{NLNL}	$(\frac{M^*}{L})^{disk}_{NLNL}$	$(\frac{M^*}{L})^{bulge}_{NLNL}$	χ^2_{MOND1}	$(\frac{M^*}{L})^{disk}_{MOND1}$	$(\frac{M^*}{L})^{bulge}_{MOND1}$
NGC 801	12.69	1.1^*	0.7	17.72	2.2^*	1.1
NGC 2998	2.22	0.6	0.8	2.50	1.2	1.3
NGC 5371	6.34	0.8	1.0	9.96	1.7^*	1.6
NGC 5533	0.98	0.7	2.2	2.12	0.1	3.7
NGC 5907	3.5	1.8	3.2	2.80	4.1^*	3.6
NGC 6674	6.32	0.4	1.8	10.83	1.5	2.9
UGC 2885	2.07	0.8	1.1	2.80	1.5^*	1.4

Table 2. Same as Table 1, for seven bulged galaxies. Disks and bulges have different M_*/L ratios. One galaxy in NLNL model and four in MOND1's predict untenably smaller M_*/L for the bulge than for the disk. These are marked by asterisks.

Galaxy	χ^2_{NLNL}	$(\frac{M^*}{L})_{0,NLNL}$	m_{NLNL}	χ^2_{MOND1}	$(\frac{M^*}{L})_{0,MOND1}$	m_{MOND1}
M 33	37.4	0.4	-0.01	27	0.6	0.01
DDO 168	20.19	0.1	-0.02	10	0.1	0.07
NGC 801	14.15	0.8	0.00	19.88	1.1	0.01

Table 3. Linear, $M_*/L = (M_*/L)_0 + mr$, fit for 3 cases not well explained neither by our formalism nor by that of MOND. Comparison with constant M_*/L of these galaxies (Table 1) shows no significant improvement.

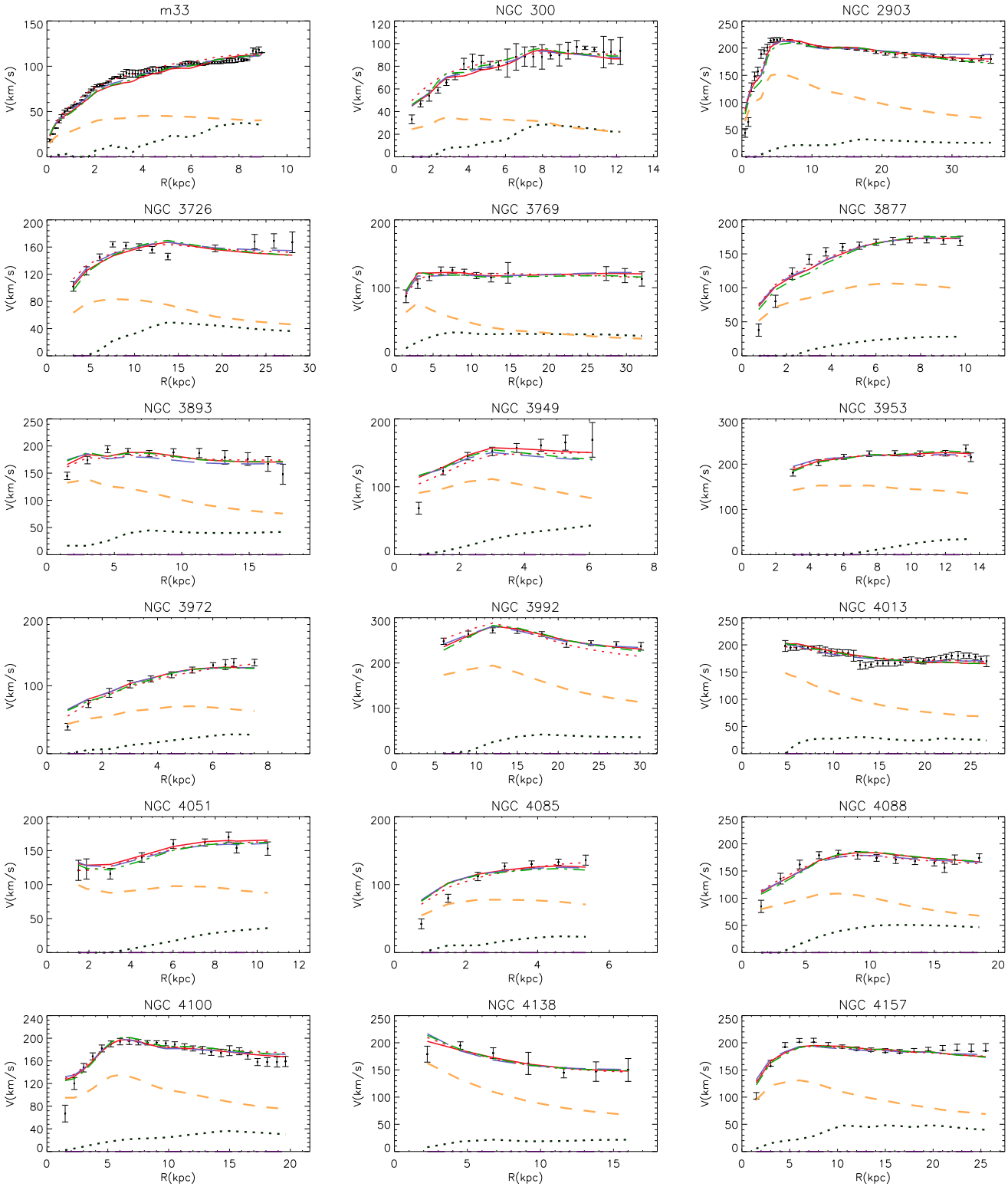

Fig. 1. Rotation curves of 32 mainly HSB galaxies. Points with vertical error bars are the observed data. Dotted (black) and short dashed lines are contributions of the gaseous and stellar components to the Newtonian rotation speeds, respectively. M_*/Ls of NLNL model are used in plotting the stellar component. Solid line is the rotation curve constructed through NLNL model. Long dashed (blue) line is that of MOND1. **Dashed-dotted (green) and dotted (red) lines are that of MOG and NFW models, respectively.**

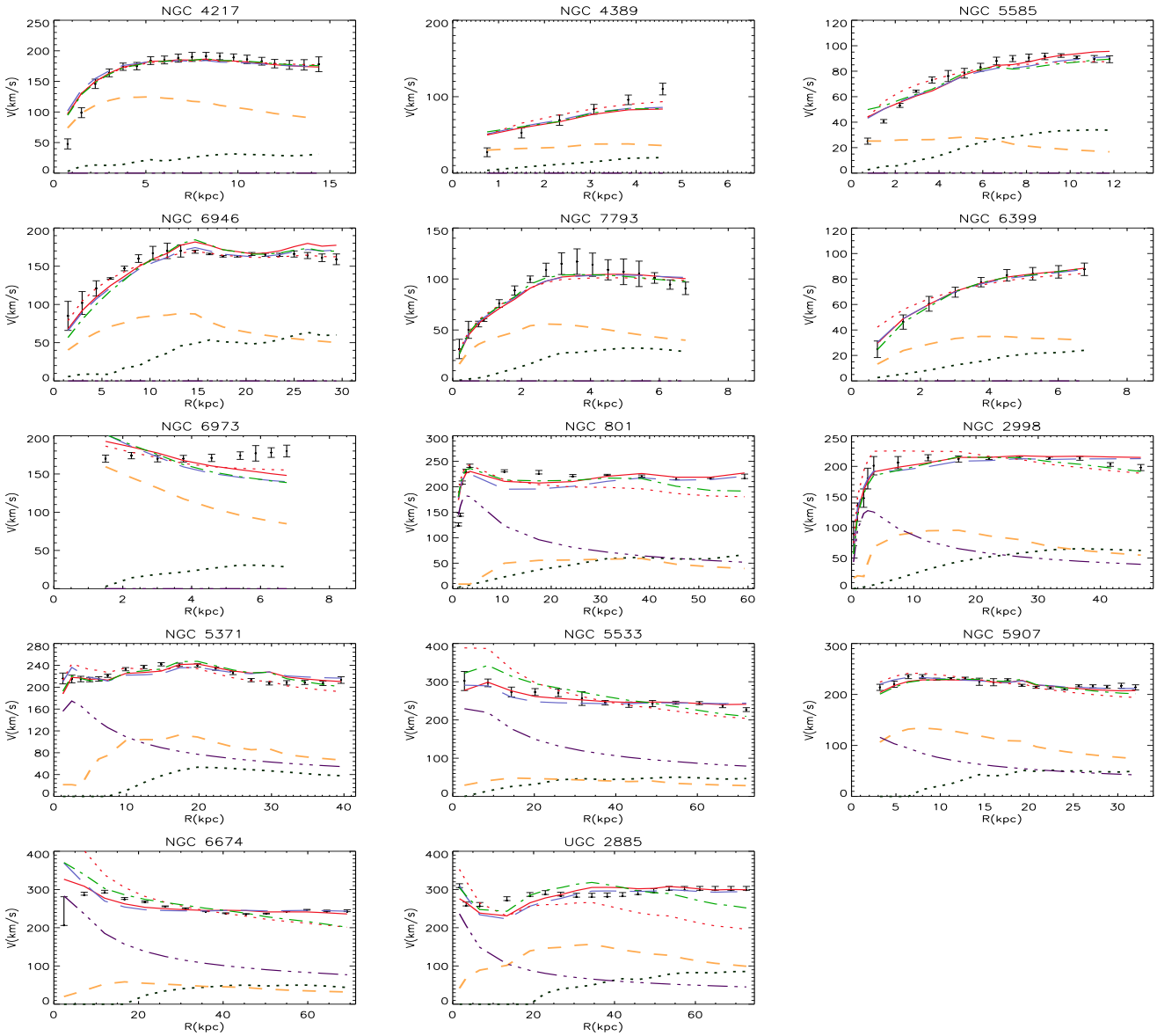

Fig. 2. Fig. 1 continued. The last seven galaxies have a bulge component, depicted as dashed-dotted lines.

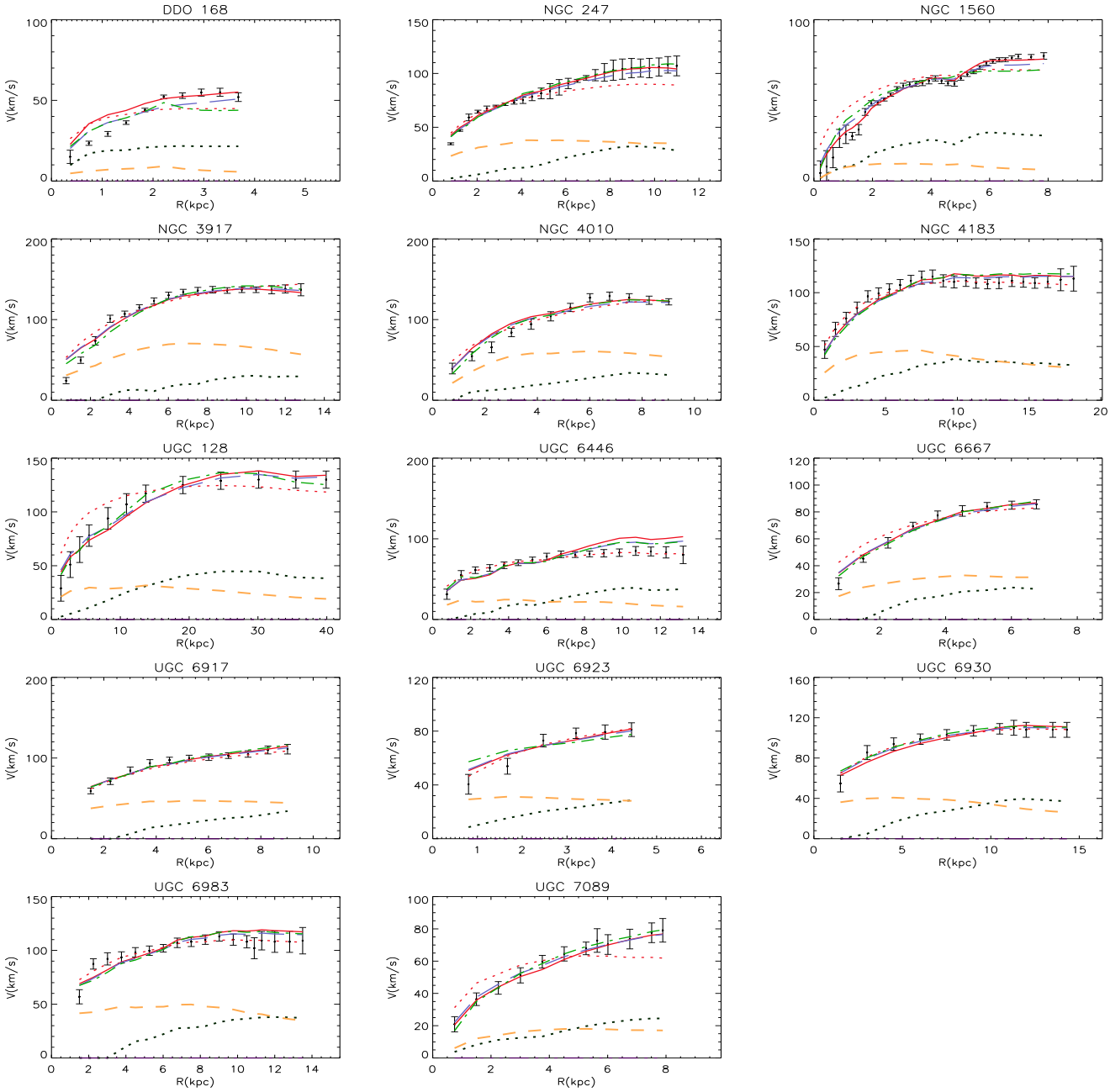

Fig. 3. Rotation curves of 14 LSB galaxies. Legend as in Fig. 1.

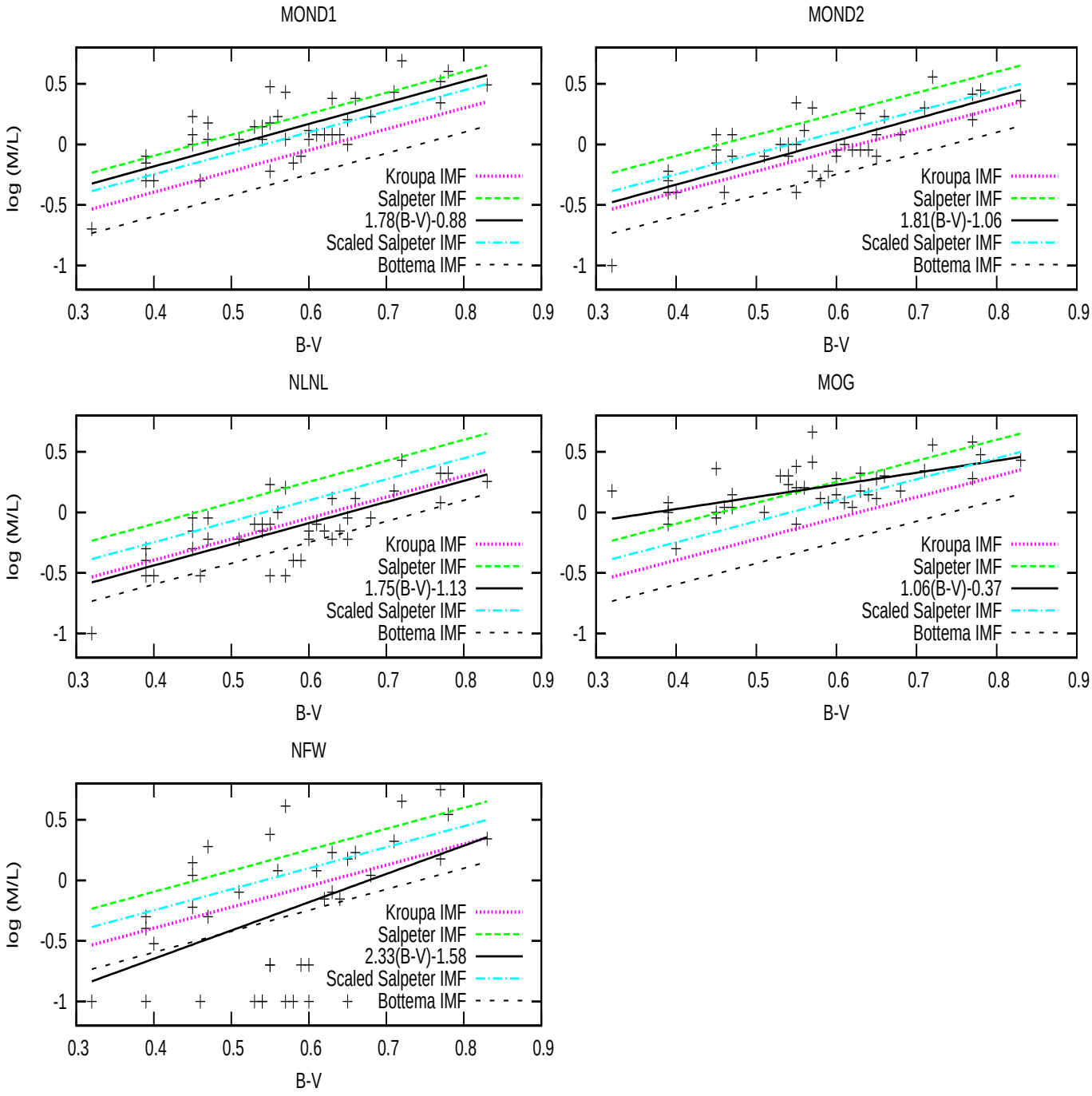

Fig. 4. Plots of M_*/L versus $B-V$. Data points in different panels are those of MOND, of NLNL, of MOG, and of CDM **with NFW halo profile**. MOND1 and MOND2 refer to the two interpolating functions, μ_1 and μ_2, of Eqs. (2) and (3), respectively. Solid line in each panel is the best fit to the prediction of the gravity model in question. Slopes and y-intercepts of best-fitted lines are shown in the panels. In NLNL and MOND, error in y-intercepts, $\sim \pm 0.15$, is small enough to distinguish one model from the other and one IMF from the other. Other lines denote the theoretical predictions of SPS with different IMFs (Bell & de Jong 2001, Bell et al. 2003). They have almost the same slope but different y-intercepts. Slopes of NLNL and MOND are reasonably close to the prediction of SPS. **That of MOG is not. Slope in NFW model is consistent with SPS prediction within the error ($\sim \pm 0.7$), but it shows large dispersion.**